MATERIALS CHARACTERIZATION 61 (2010) 992–999

available at www.sciencedirect.com

ScienceDirect

www.elsevier.com/locate/matchar

Mössbauer spectroscopy study on the corrosion resistance of plasma nitrided ASTM F138 stainless steel in chloride solution

S.D. de Souza[a], M. Olzon-Dionysio[a,*], R.L.O. Basso[b], S. de Souza[c]

[a]Departamento de Física, Universidade Federal de São Carlos, 13565-950, São Carlos, SP, Brazil
[b]Centro de Ciências Exatas e Tecnologia, Universidade de Caxias do Sul, 95070-560, Caxias do Sul, RS, Brazil
[c]Instituto de Pesquisas Energéticas e Nucleares, 05422-970, São Paulo, SP, Brazil

ARTICLE DATA

Article history:
Received 24 September 2009
Received in revised form
18 June 2010
Accepted 18 June 2010

Keywords:
ASTM F138 stainless steel
Plasma nitriding
Mössbauer spectroscopy
Glancing angle X-ray diffraction
Corrosion

ABSTRACT

Plasma nitriding of ASTM F138 stainless steel samples has been carried out using dc glow discharge under 80% H_2–20% N_2 gas mixture, at 673 K, and 2, 4, and 7 h time intervals, in order to investigate the influence of treatment time on the microstructure and the corrosion resistance properties. The samples were characterized by scanning electron microscopy, glancing angle X-ray diffraction and conversion electron Mössbauer spectroscopy, besides electrochemical tests in NaCl aerated solution. A modified layer of about 6 μm was observed for all the nitrided samples, independent of nitriding time. The X-ray diffraction analysis shows broad γ_N phase peaks, signifying a great degree of nitrogen supersaturation. Besides γ_N, the Mössbauer spectroscopy results indicated the occurrence of γ' and ε phases, as well as some other less important phases. Corrosion measurements demonstrate that the plasma nitriding time affects the corrosion resistance and the best performance is reached at 4 h treatment. It seems that the ε/γ' fraction ratio plays an important role on the resistance corrosion. Additionally, the Mössbauer spectroscopy was decisive in this study, since it was able to identify and quantify the iron phases that influence the corrosion resistance of plasma nitrided ASTM F138 samples.

1. Introduction

Considerable progress has been made in the improvement and development of prosthetic devices intended for implantation in the human body. Compatibility, or the absence of body reaction, is one of the major problems associated with metal implants. Generally, metallic components that are used for orthopedic applications for bone repairing and replacement could fail mechanically due to corrosion damage. The corrosion of the metallic piece implanted in the human body may lead to the release of corrosion products in the biological fluids. These corrosion products may provoke tissue irritation or infection [1–3].

Nowadays, F138 stainless steel implants are widely used in the field of orthopedic applications, although biological complications may result from inadequate mechanical and tribological properties [4,5].

In order to reduce corrosion and wear rates of the biomaterials, as well as to increase their fatigue strength, several efficient treatments are used such as anodization, passivation, and others [6]. In addition to these processes, plasma nitridind has been widely used as surface treatment on stainless steels samples [7–10]. Plasma nitriding is a common surface treatment in which nitrogen is introduced into the metal in order to improve the durability of mechanical parts and it has been successfully applied in the nuclear and mechanical engineering industries with respect to corrosion, wear, hardness and fatigue resistance [3,7–15].

The mechanical and tribological properties as well as the corrosion resistance of nitrided samples are strongly related

* *Corresponding author*. Tel./fax: +55 16 3361 4835.
E-mail address: dmod@df.ufscar.br (M. Olzon-Dionysio).

1044-5803/$ – see front matter © 2010 Elsevier Inc. All rights reserved.
doi:10.1016/j.matchar.2010.06.015

to the phase formed during treatment [16–18]. At relatively high temperatures (773 K or above), the nitriding can improve hardness and wear resistance; while the corrosion resistance is usually diminished due to the formation of a very stable and hard precipitate chromium nitride (CrN) [13,14]. Depletion of chromium in the metal matrix zone prevents the formation of a uniform and protective passive film and the metal surface is therefore subjected to active corrosion [17]. At temperatures lower than about 723 K, the chromium diffusion is reduced and, consequently, the formation of chromium nitride is inhibited [14]. Using low treatment temperatures, the modified surface layer mainly consists of a metastable phase known as expanded austenite or supersaturated nitrogen solid-solution FCC phase, besides a cubic phase (γ'-Fe_4N), and a hexagonal phase (ε-$Fe_{2-3}N$). The metastable phase is known as expanded austenite γ_N phase [19], S phase [20], or *m* phase [21] and it has been identified as the primary reason for the increase in the mechanical and tribological properties, as well as corrosion resistance [22,23]. Recent work pointed that the γ_N phase is formed by two magnetic phases, depending on the nitrogen concentration [24].

However, a recent study of plasma nitrided AISI 316 L samples [15], which used, among other analysis techniques, Mössbauer Spectroscopy, produced an empirical model to improve the corrosion resistance. This resistance seems to be more related to the ε/γ' fraction ratio than to the γ_N phase. The sample which presented the best result for corrosion, also presented the maximum value for this ratio. Mössbauer results were decisive in this study, since it is a powerful tool to both identify and quantify different phases (containing Fe) with accuracy. So, corrosion research in steels is an area in which Mössbauer spectroscopy has become a required analytical technique [25].

In this work, an investigation on ASTM F138 stainless steel is presented. The plasma nitriding technique was used for nitriding the samples, at 673 K, during different time intervals, in order to investigate the influence of this parameter on the morphology, composition and corrosion protection behavior of the modified layers. Therefore, the main purpose of this research is to test out the empirical model used on a similar, system and published elsewhere [15].

2. Materials and Methods

In this study, we used the ASTM F138 stainless steel, a stainless steel used as biomaterial, produced by Villares Metals. The stainless steel was annealed by the manufacturer at 1323 K for 60 min and then cooled in water. Its chemical composition (in wt.%) is: Cr (18.40), Ni (14.01), Mo (2.46), C (0.022), and Fe balance. The samples [diameter: 2.0 cm, thickness: 0.3 cm] were polished, cleaned ultrasonically in acetone and finally air-dried. Next, they were plasma nitrided in equipment with a D.C. power supply, similar to that described by Hudis [26].

A conventional dc glow discharge was applied with the following parameters: 80% H_2–20% N_2, pressure of about 6 mbar. Voltage (~450 V) and current density (~500 mA) were adjusted to maintain the cathode temperature (or nitriding temperature, T_N=673 K), at different nitriding time intervals (t_N) of 2, 4, and 7 h.

Glancing Angle X-ray Diffraction (GAXRD) and Conversion Electron Mössbauer Spectroscopy (CEMS) analyses were performed to identify the phases formed during plasma nitriding.

The GAXRD measurements were performed in two configurations: First, the measurements were made using a Siemens D5000 diffractometer with Cu Kα radiation. The conditions were: a 2θ scan step of 0.03°, ranging from 35° to 85°, an angle of incidence fixed at 3° and 4 s of counting time.

The second series of measurements was performed on the D12A-XRD1 beam line at the Brazilian Synchrotron Light Laboratory (LNLS – Campinas). The experimental conditions were: wavelength lambda=0.20836213 nm, pyrolytic graphite analyzer at the diffracted beam, scintillation counter, incidence angle fixed at 3°, 2θ ranging from 40° to 140° in 0.1° 2θ steps. The Mössbauer spectra of untreated and nitrided samples were obtained in the backscattering geometry, using a conventional constant acceleration Mössbauer spectrometer. A homemade detection chamber was used, with a 95% He+5% CH_4 gas mixture flux. A ^{57}Co source in Rh matrix with nominal activity of 25 mCi was used. The CEMS measurements were performed at room temperature, and the isomer shifts are given relative to α–Fe.

The corrosion performance of the samples was investigated in 3% NaCl aerated electrolytic solution using a EG&G 273A Potentiostat/Galvanostat. Potentiodynamic polarization curves were obtained using the EG&G-Pal M352 Software. The scanning potential was in the range of −1.0 V(SCE) (cathodic potential) to +1.2 V(SCE) (anodic potential), and the scan rate was 1 mVs^{-1}. Electrochemical experiments were performed in a conventional Pyrex cell using untreated and nitrided ASTM F138 samples as working electrodes and a platinum sheet as counter electrode. The potentials were referred to the saturated calomel electrode (SCE) in a KCl solution and all the electrochemical experiments were performed at room temperature. After the corrosion tests, microstructural analysis was carried out in order to evaluate the corrosion morphology and the extent of damage, using a JEOL scanning electron microscope, JSM – 5800 LV model.

3. Results and Discussion

3.1. *Characterization of Plasma Nitrided Layer*

3.1.1. *Scanning Electron Microscopy (SEM) and GAXRD results*

All the nitrided samples presented very similar SEM micrographs, independent of the nitriding time. This behavior was observed before, for 316 L samples [15], nitrided under the same conditions. Fig. 1 shows the SEM micrograph for the sample nitrided for 7 h. The thickness (d) of the compound layer, about 6 μm, can be visually estimated from this figure, while the 316 L samples were approximately 8 μm thick.

Figs. 2 and 3 show the GAXRD diffractograms of the samples, before and after nitriding, during different time intervals, measured using laboratory equipment and a synchrotron radiation, respectively.

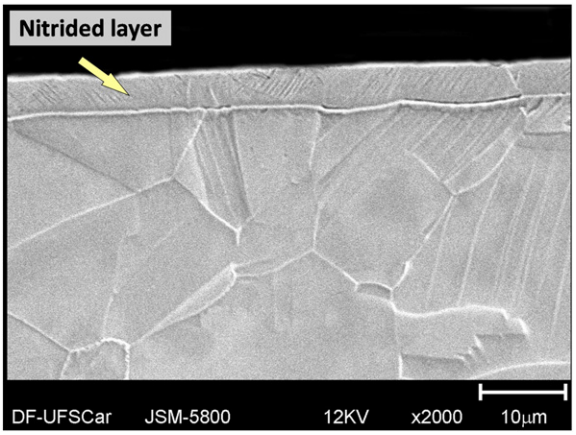

Fig. 1 – SEM micrograph for the ASTM F138 sample nitrided during 7 h.

Although the measurements with different energies do not reach the same depth, approximately 0.7 μm for Fig. 2 and 2.0 μm for Fig. 3 [27], the following can be observed: The nitrided samples show broad γ_N phase whose peaks are shifted to lower angles than untreated samples positions. It suggests a great degree of nitrogen supersaturation, indicating that the nitrided layers, which are formed are rich in defects and are highly stressed [28]. Moreover, for t_N=7 h, the γ_N phase peaks approach the ones of untreated sample positions, which indicates that this sample may present a lower concentration of nitrogen [7].

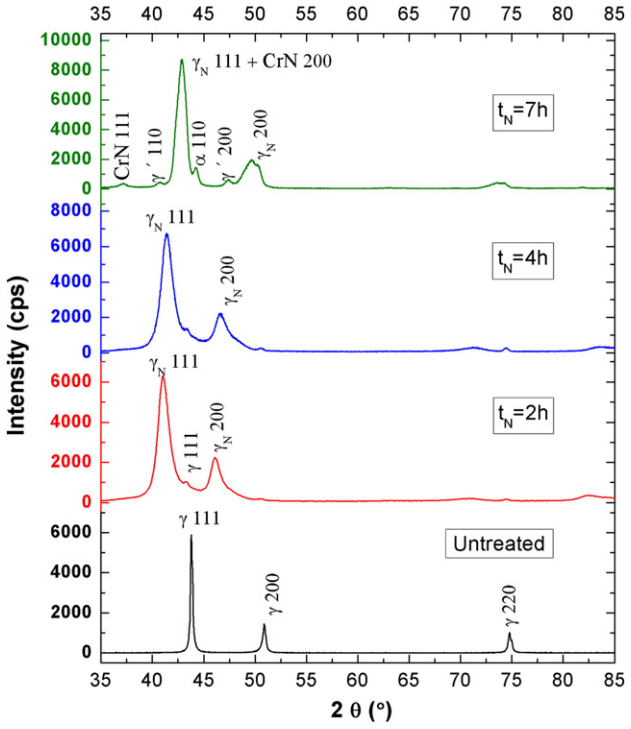

Fig. 2 – GAXRD diffractograms for the ASTM F138 samples, before and after nitriding, during different time intervals t_N using a conventional diffractometer.

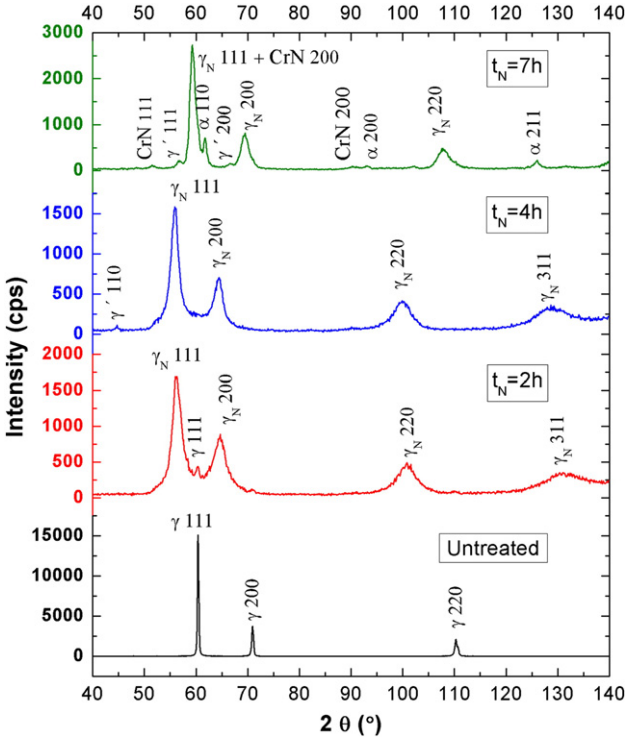

Fig. 3 – GAXRD diffractograms for the ASTM F138 samples, before and after nitriding, during different time intervals t_N using the synchrotron radiation diffraction.

It seems difficult to confirm the presence of the γ′ phase for nitriding time t≤4 h because of the proximity of its peak positions and the γ_N phase peaks. However, the γ′ peaks appear on the sample nitrided for 7 h. Besides, the CrN and α phase traces can also be seen on the LNLS diffractogram, as Fig. 4 shows.

As a temperature of 673 K was used to avoid the formation of CrN, its presence can seem unusual. However, if temperature exceeds 693 K, the solubility limit of nitrogen in austenitic structure is reached, the metastable γ_N phase is decomposed, and precipitation of Cr nitrides occurs, which is relatively stable [29]. The temperature possibly reached this value in sample borders, due to the edge effects [30].

3.1.2. *Conversion Electron Mössbauer Spectroscopy (CEMS)*

CEMS measurements of the surface layer (up to the depth of 0.5 μm [31]) are related to compounds that contain Fe (in the present case) or other atoms, according to the source.

Fig. 5 shows the Mössbauer spectrum for the sample before nitriding. The analysis of this spectrum shows the following: the surface of the untreated sample is formed by 47% of austenitic f.c.c. phase represented by one single-line (isomer shift IS=−0.10(1) mm/s). The remaining 53% is represented by one double-line component (IS=−0.09(1) mm/s and quadrupole splitting EQ=0.12(1) mm/s), which means that the FCC cubic symmetry is affected by the Fe atom neighbors. These hyperfine parameters are in good agreement with previous results [32].

Fig. 6 shows the CEMS data for the samples nitrided at 2, 4 and 7 h.

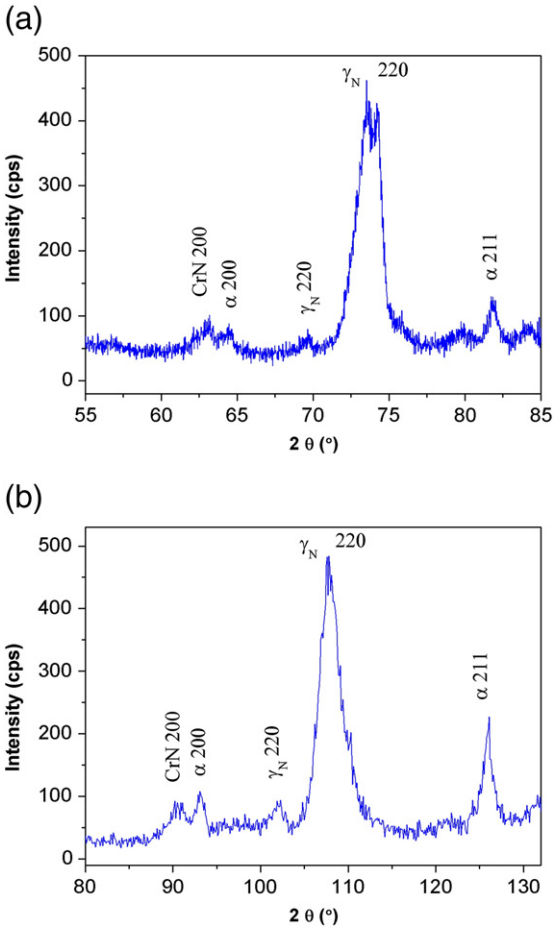

Fig. 4 – Zoom of diffractograms (t_N = 7 h), from Fig. 2(a) and Fig. 3(b).

These spectra were fitted as a superposition of sub-spectra corresponding to different phases: the γ′(Fe_4N), a nitrogen supersaturated solid phase γ_N, a hexagonal ε phase ($Fe_{2+x}N$) and a last multiple phase, α*.

The present γ_N phase shows both characteristics, paramagnetic (γ_N(p)) and magnetic (γ_N(m)). The γ_N(m) phase contains more N in solution than the γ_N(p) phase [24,33]. On the other hand, the α* phase is a superposition of multiple sextets

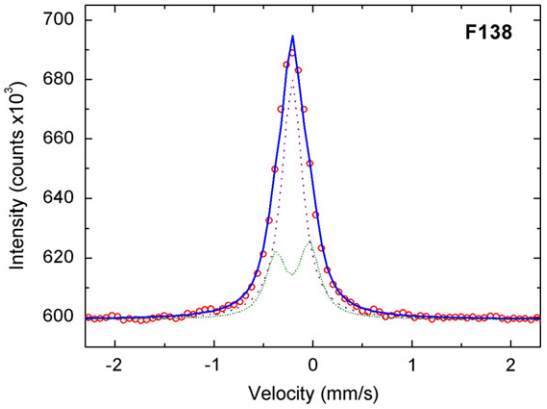

Fig. 5 – CEMS data for the ASTM F138 sample before nitriding.

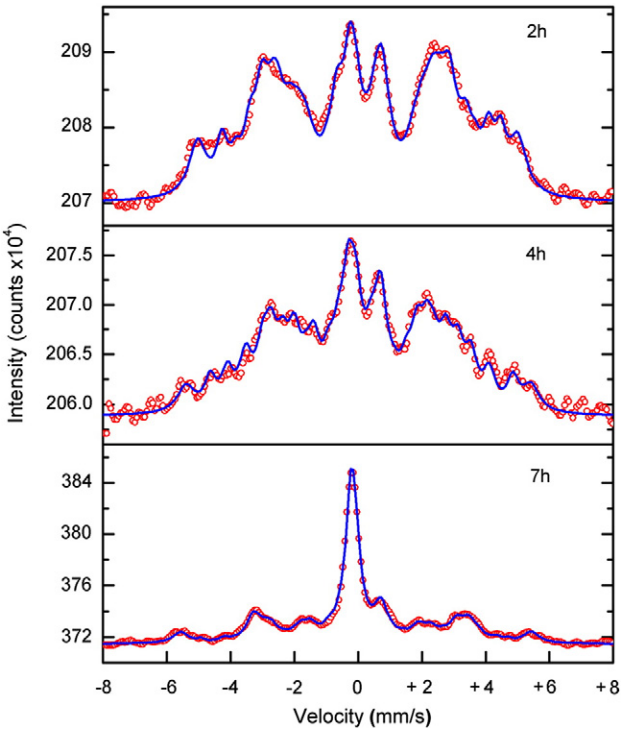

Fig. 6 – CEMS data for the ASTM F138 samples nitrided at t_N = 2, 4 and 7 h.

referring to α(Fe,Cr,Ni), α′-martensite and α″-$Fe_{16}N_2$ phases, which are probably the consequence of induced stress during the N implantation [34].

Table 1 presents the range of values of the Mössbauer parameters used for the samples nitrided for different times. These parameters are similar to those previously published [34–41].

Fig. 7 shows the phase fractions obtained from the Mössbauer fits as a function of nitriding time, where $\gamma_N = \gamma_N$(p) + γ_N(m). While the γ′ phase concentration stays almost constant, (35 ± 4), the ε phase concentration seems to be correlated with the γ_N phase. If the γ_N fraction decreases (increases), the ε fraction increases (decreases).

Table 1 – Range of values of the hyperfine parameters used to fit the different CEMS spectra for nitriding time (t_N) of 2, 4, and 7 h. H is the magnetic hyperfine field, EQ is the quadrupole splitting, IS is the isomer shift.

Phase	H (T)	EQ (mm/s)	IS (mm/s)
γ_N (m)	17.5 ± 0.5	–	0.11 ± 0.07
γ_N (m)	12.8 ± 0.3	–	0.25 ± 0.03
ε-$Fe_{2.02}N$	–	0.36 ± 0.02	0.35 ± 0.04
γ′-Fe_4N	34.0 ± 0.1	–	0.20 ± 0.05
	21.5 ± 0.5	0.23 ± 0.11	0.20 ± 0.04
	21.4 ± 0.5	−0.18 ± 0.01	0.29 ± 0.05
γ_N(p)	–	–	−0.21 ± 0.03
ε-$Fe_{2+x}N$			
x = 0.60 (7), 1.2	26.4 ± 3.0	–	0.23 ± 0.14
	11.0 ± 0.1	–	0.37 ± 0.01
α*	29.5 ± 4.0	–	−0.01 ± 0.09

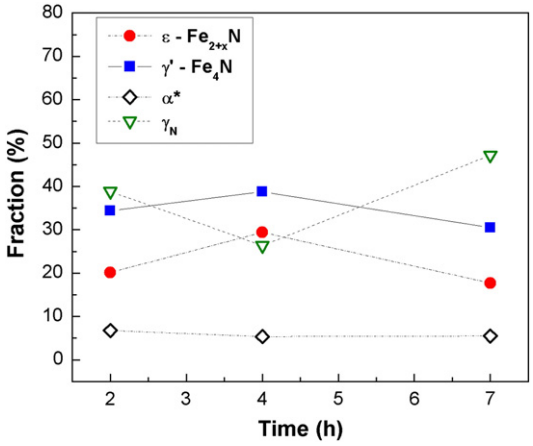

Fig. 7 – Fractions of the adjusted phases as a function of different time intervals t_N. The solid lines are a guide for the eye.

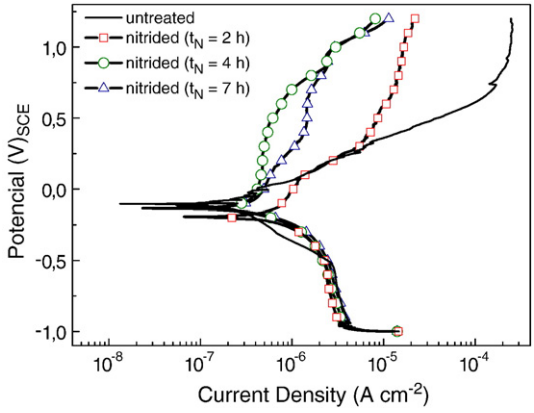

Fig. 8 – Polarization curves in 3% NaCl aerated electrolytic solution of the ASTM F138 samples untreated and nitrided at t_N=2, 4 and 7 h.

As CEMS results can reveal the behavior of the magnetic nature of the γ_N phase, it is interesting to discuss it from the point of view of nitriding time. Table 2 shows the relative fraction for the paramagnetic (γ_N(p)) and magnetic (γ_N(m)) phases for different nitriding times.

If the nitriding time increases, the results indicate that the γ_N (m) phase (or N concentration) decreases and the paramagnetic γ_N (p) phase increases. This situation was observed for 316 L [15], and it had been observed before, when the γ_N (m) phase (produced in 304 Stainless steel) transformed systematically on annealing at 673 K to a thicker γ_N (p) phase with less N in solution and less lattice expansion, thereby destabilizing the magnetic state of the γ_N (m) [35]. The result for t_N=7 h is compatible with the corresponding GAXRD, which indicated a lower concentration in this sample.

3.2. *Corrosion Behavior*

The potentiodynamic polarization curves from the linear voltammetry of untreated and nitrided samples are shown in Fig. 8. From these curves, the corrosion potential (E_{corr}) and the highest anodic current density (j_{ha}) values are given in Table 3.

In Fig. 8, the potentiodynamic curves indicate that samples nitrided at different time intervals present a significant decrease in the anodic dissolution current in comparison with the untreated samples' reference curve. The anodic current densities of the curves for the samples nitrided at 2 and 7 h are shifted by about one order of magnitude towards smaller values with respect to the untreated sample. Meanwhile, the curve of treated sample, especially in the case of the sample nitrided for 4 h, shows a large shift to smaller anodic currents, by about two orders of magnitude towards smaller values than the reference curve. It means that the metal surface becomes less reactive due to the plasma nitriding treatment and, as a consequence, the anodic dissolution currents decrease during the anodic sweep. The surface that was plasma nitrided for 4 h is less reactive than the surfaces plasma nitrided for 2 or 7 h, but all of these samples are less reactive than the untreated surface. In particular, in Fig. 8, the potentiodynamic curve obtained for the untreated electrode shows, at approximately −0.10 to 0.0 V (SCE), a more intense fluctuation of frequency potential. This potential fluctuation can be due to the difficulty of passive film formation and, posterior pit nucleation phenomena because of the attack of chloride ions in the environment. In this region of the potentiodynamic curve, an increase of dissolution current with increasing potential is observed. Starting at approximately 0.0 until +1.2 V(SCE), the anodic behavior of the matrix in NaCl solution is represented by a curve with a high active dissolution rate, which increases anodic current values with increasing potential. This last potential interval transpassive, where the dissolution rate again increases with increasing potential, is apparently due to the destruction of the passive film, indicating localized corrosion or pitting corrosion.

The morphological analysis, which was carried out on the surface of nitrided samples after the corrosion tests, is in agreement with the electrochemical tests. The amount and sizes of pits can be clearly seen in the SEM micrographs shown

Table 2 – Paramagnetic and magnetic γ_N phases relative fraction for different times t_N.

Time t_N (h)	γ_N (p) (%)	γ_N (m) (%)	$\gamma_{N=}\gamma_N$ (p) + γ_N (m) (%)
2	5	34	39
4	10	16	26
7	35	17	52

Table 3 – Corrosion potential and highest anodic current density values from polarization curves obtained in 3% NaCl aerated electrolytic solution for ASTM F138 samples untreated (t_N=0 h) and nitrided at different times t_N.

Time t_N (h)	Highest anodic current density ≅ j_{ha} 10^{-4} (A cm^{-2}),	Corrosion potential ≅ E_{corr} ($V_{(SCE)}$)
0	2.55	−0.10
2	0.221	−0.19
4	0.081	−0.14
7	0.114	−0.14

in Fig. 9(a)–(d). The sample nitrided during 4 h (Fig. 9(c)), which had a lower anodic dissolution current, shows considerably fewer number of pits regarding the other samples (Fig. 9(a),(b) and (d)). These results and the observations above suggested that the treatment time of 4 h improved the corrosion resistance of stainless steel in NaCl solution since the nitrided layer that was formed in this sample shows the strongest passive character.

To better understand this behavior, it is interesting to examine Table 4, where it can be seen that this sample (4 h) presents a maximum value not only for the γ' phase, but for the ε phase as well. Although they could be considered responsible for the improvement, the fact that it did not happen in the previous study on 316 L [15], a correlation between the best response for corrosion resistance and the ratio between ε and γ' is suggested. The last column of Table 4 illustrates this correlation: the higher the ratio, the better the corrosion resistance is.

Jirásková et al. [36] studied the effect of the nitrogen uptake in α-iron upon different methods (spark erosion in gaseous and liquid ammonia, plasma nitriding, and plasma immersion ion implantation). They observed that the presence of the ε phase influences the deterioration of the samples. However, this influence was not clear, because for one method, this phase favored the damage and for the other one, it seemed to prevent it. It is worth noting that the γ' phase appeared after different annealing treatments in the samples of this last method. So, their results seem to indicate that the presence of γ' phase might reduce the deterioration.

Table 4 – Phases fractions obtained from the Mössbauer fits as a function of nitriding time t_N.

Time t_N (h)	γ_N (%)	α^* (%)	ε-$Fe_{2+x}N$ (%)	γ' (%)	ε/γ' fraction ratio
2	39	7	21	33	0.64
4	26	5	30	39	0.77
7	52	2	15	31	0.48

On the other hand, some authors [14] have regarded the presence of the γ_N phase as being responsible for better corrosion resistance. However, when the behavior of this phase in Table 4 is observed, it might not be responsible for better corrosion resistance, as it presents a minimum value for t=4 h. However, it is possible that this phase has a certain importance in the corrosion resistance. We are currently developing a systematic study using a higher number of

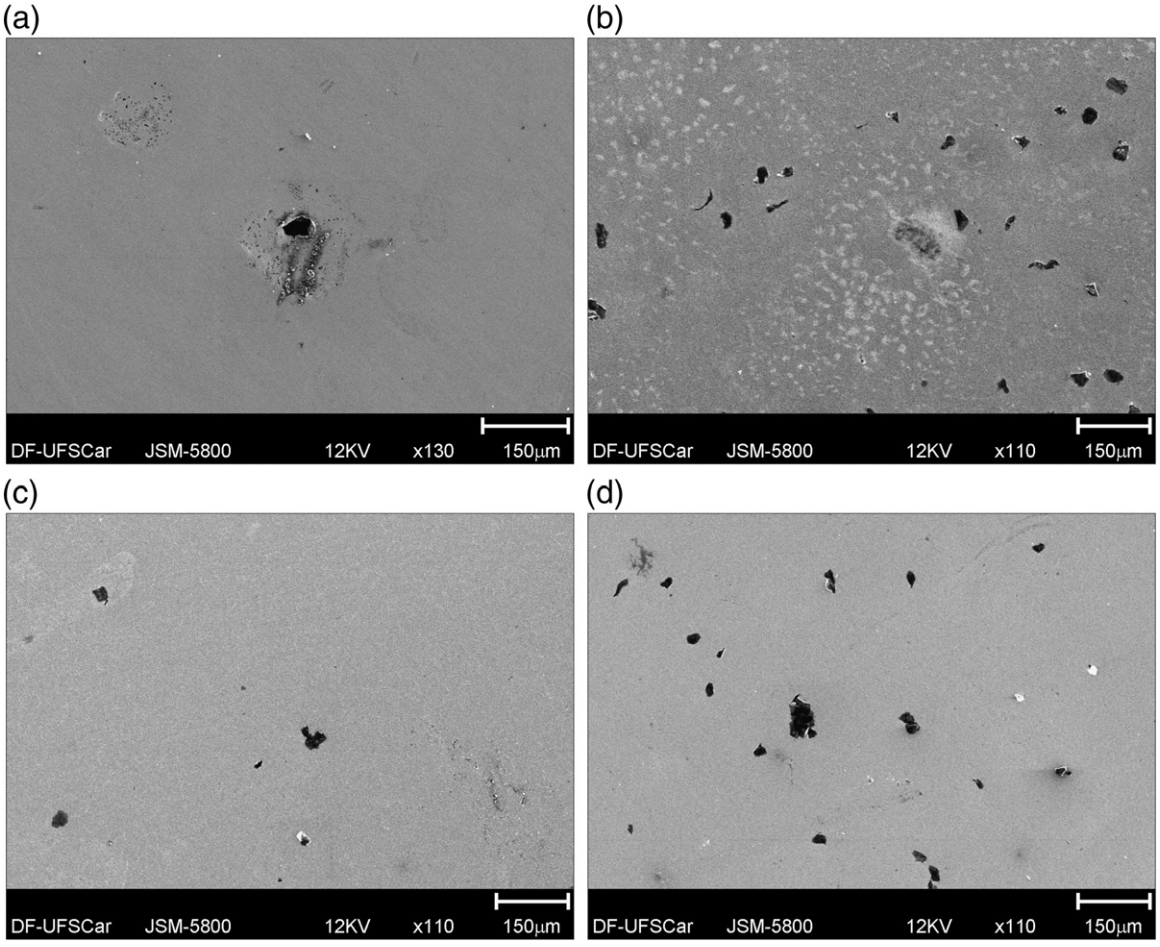

Fig. 9 – SEM micrographs of the ASTM F138 samples after corrosion tests: untreated (a) and nitrided at t_N=2 h (b), 4 h (c), and 7 h (d).

samples, with the aim of improving this empirical model, also considering this phase.

4. Conclusions

The dc glow discharge plasma nitriding produced a modified layer on the surface of the austenitic substrate, whose thickness, about 6 μm, does not seem to depend on the nitriding time.

The GAXRD analysis shows the presence of a broad γ_N phase whose peaks appear at lower angles, suggesting a great degree of nitrogen supersaturation. As the nitriding time increases, the shift of γ_N phase peaks decreases, as well as their full widths at half maximum, indicating that the N concentration decreases.

The CEMS analysis indicated the occurrence of γ' and ε phases, as well as γ_N and other less important phases. Concerning the γ_N phase's magnetic character, the results indicate that as the nitriding time increases, a significant reduction in the relative fraction of the γ_N (m) phase is observed and the paramagnetic γ_N (p) phase, (that presents less nitrogen), also increases, which confirmed the GAXRD results.

Corrosion measurements demonstrate that the processing time during the plasma nitriding treatment plays an important role in the corrosion resistance of ASTM F138 after nitriding.

The results suggest that the plasma nitriding treatment time of 4 h improved the corrosion resistance, while the sample nitrided for the longest time (t_N=7 h) exhibits lower corrosion resistance. It seems that the ε/γ' fraction ratio plays an important role in the resistance corrosion. The ASTM F 138 nitrided sample (t_N=4 h) which presented the best result for corrosion, also presented the maximum value for this ratio.

The Mössbauer spectroscopy was decisive in this study, since it could identify and quantify the iron phases that seem to affect the corrosion resistance of plasma nitrided ASTM F138 samples.

Acknowledgments

The Brazilian agencies FAPESP and CAPES gave financial support for this investigation. The authors would like to thank Dr. L. M. Galego from IPEN (Brazil) for the LNLS measurements and discussions.

REFERENCES

[1] Bordji K, Jouzeau J-Y, Mainard D, Payan E, Delagoutte J-P, Netter P. Evaluation of the effect of three surface treatments on the biocompatibility of 316L stainless steel using human differentiated cells. Biomaterials 1996;17:491–500.
[2] Shettlemore MG, Bundy KJ. Examination of in vivo influences on bioluminescent microbial assessment of corrosion product toxicity. Biomaterials 2001;22:2215–28.
[3] Liu CL, Chu PK, Lin GQ, Qi M. Anti-corrosion characteristics of nitride-coated AISI 316L stainless steel coronary stents. Surf Coat Technol 2006;201:2802–6.
[4] Liang H, Shi B, Fairchild A, Cale T. Applications of plasma coatings in artificial joints: an overview. Vacuum 2004;73:317.
[5] Wilches LV, Uribe JA, Toro A. Wear of materials used for artificial joints in total hip replacements. Wear 2008;265: 143–9.
[6] Baptista CARP, Schneider SG, Taddei EB, da Silva HM. Fatigue behavior of arc melted Ti–13Nb–13Zr alloy. Int J Fatigue 2004;26:967–73.
[7] Picard S, Memet JB, Sabot R, Grosseau-Poussard JL, Rivière JP, Meilland R. Corrosion behaviour, microhardness and surface characterisation of low energy, high current ion implanted austenitic stainless steel. Mater Sci Eng 2001;A303:163–72.
[8] Liang W. Surface modification of AISI 304 austenitic stainless steel by plasma nitriding. Appl Surf Sci 2003;211:308–14.
[9] Li CX, Bell T. Corrosion properties of plasma nitrided AISI 410 martensitic stainless steel in 3.5% NaCl and 1% HCl aqueous solutions. Corros Sci 2006;48:2036–49.
[10] Shokouhy A, Larijani MM, Ghoranneviss M, Haji Hosseini SH, Yari GM, Sari AH, et al. Microstructural and corrosivity changes induced by nitrogen ion implantation on chromium films. Thin Solid Films 2006;515:571–5.
[11] Li CX, Bell T. Corrosion properties of active screen plasma nitrided 316 austenitic stainless steel. Corros Sci 2004;46: 1527–47.
[12] Fossati A, Borgioli F, Galvanetto E, Bacci T. Glow-discharge nitriding of AISI 316L austenitic stainless steel: influence of treatment time. Surf Coat Technol 2006;200:3511–7.
[13] Borgioli F, Fossati A, Galvanetto E, Bacci T. Glow-discharge nitriding of AISI 316L austenitic stainless steel: influence of treatment temperature. Surf Coat Technol 2006;200: 2474–80.
[14] Fossati A, Borgioli F, Galvanetto E, Bacci T. Corrosion resistance properties of glow-discharge nitrided AISI 316L austenitic stainless steel in NaCl solutions. Corros Sci 2006;48: 1513–27.
[15] Olzon-Dionysio M, de Souza SD, Basso RLO, de Souza S. Application of Mössbauer spectroscopy to the study of corrosion resistance in NaCl solution of plasma nitrided AISI 316L stainless steel. Surf Coat Technol 2008;202:3607–14.
[16] Blawert C, Weisheit A, Mordike BL, Knoop FM. Plasma immersion ion implantation of stainless steel: austenitic stainless steel in comparison to austenitic–ferritic stainless steel. Surf Coat Technol 1996;85:15–27.
[17] Mingolo N, Tschiptschin AP, Pinedo CE. On the formation of expanded austenite during plasma nitriding of an AISI 316L austenitic stainless steel. Surf Coat Technol 2006;201:4215–8.
[18] Basso RLO, Candal RJ, Figueroa CA, Wisnivesky D, Alvarez F. Influence of microstructure on the corrosion behavior of nitrocarburized AISI H13 tool steel obtained by pulsed DC plasma. Surf Coat Technol 2009;203:1293–7.
[19] Samandi M, Sheden BA, Smith DI, Collins CA, Hutchings R, Tendys J. Microstructure, corrosion and tribological behaviour of plasma immersion ion-implanted austenitic stainless steel. Surf Coat Technol 1993;74–75:261–6.
[20] Bacci T, Borgioli F, Galvanetto E, Pradelli G. Glow-discharge nitriding of sintered stainless steels. Surf Coat Technol 2001;139:251–6.
[21] Singh V, Marchev K, Cooper CV, Meletis EI. Intensified plasma-assisted nitriding of AISI 316L stainless steel. Surf Coat Technol 2002;160:249–58.
[22] Jargelius-Pettersson RFA. Electrochemical investigation of the influence of nitrogen alloying on pitting corrosion of austenitic stainless steels. Corros Sci 1999;41:1639–64.
[23] Baba H, Kodama T, Katada Y. Role of nitrogen on the corrosion behavior of austenitic stainless steels. Corros Sci 2002;44: 2393–407.
[24] Basso RLO, Pimentel VL, Weber S, Marcos G, Czerwiec T, Baumvol IJR, et al. Magnetic and structural properties of ion nitrided stainless steel. J Appl Phys 2009;105:124914–5.

[25] Cook DC. Application of Mössbauer spectroscopy to the study of corrosion. Hyperfine Interact 2004;153:61–82.
[26] Hudis M. Study of ion-nitriding. J Appl Phys 1973;44:1489–96.
[27] J. H. Hubbell and S. M. Seltzer, Tables of X-Ray Mass Attenuation Coefficients and Mass Energy-Absorption Coefficients, available at http://physics.nist.gov/PhysRefData/XrayMassCoef/cover.html.
[28] Wang L, Ji S, Sun J. Effect of nitriding time on the nitrided layer of AISI 304 austenitic stainless steel. Surf Coat Technol 2006;200:5067–70.
[29] Li G-J, Peng Q, Li C, Wang Y, Gao J, Chen S-Y, et al. Effect of DC plasma nitriding temperature on microstructure and dry-sliding wear properties of 316L stainless steel. Surf Coat Technol 2008;202:2749–54.
[30] Olzon-Dionysio M, Campos M, de Souza S, de Souza SD,. Influences of plasma nitriding edge effect on properties of 316L stainless steel. Surf Coat Technol 2010;204:3623–8.
[31] Jirásková Y, Blawert C, Schneeweiss O. Thermal stability of stainless steel surfaces nitrided by plasma immersion ion implantation. Phys Status Solidi (a) 1999;175:537–48.
[32] Cordier-Robert C, Bourdeau L, Magnin T, Foct J. Nitrogen implantation of stainless steel studied by Mössbauer spectroscopy and X-ray diffraction. J Mater Sci Lett 1994;13:352–4.
[33] Öztürk O, Williamson DL. Phase and composition depth distribution analyses of low energy, high flux N implanted stainless steel. J Appl Phys 1995;77(8):3839–50.
[34] Wei R, Vajo JJ, Matossian JN, Wilbur PJ, Davis JA, Williamson DL, et al. A comparative study of beam ion implantation, plasma ion implantation and nitriding of AISI 304 stainless steel. Surf Coat Technol 1996;83:235–42.
[35] Öztürk O, Williamson DL. Thermal stability of the high-N solid-solution layer on stainless steel. Surf Coat Technol 2002;158–159:288–94.
[36] Jirásková Y, Havlícek S, Schneeweiss O, Perina V, Blawert C. Characterization of iron nitrides prepared by spark erosion, plasma nitriding, and plasma immersion ion implantation. J Magn Magn Mater 2001;234:477–88.
[37] Firrao D, Rosso M, Principi G, Frattini R. The influence of carbon on nitrogen substitution in iron ε-phases. J Mater Sci 1982;17(6):1773–88.
[38] dos Santos CA, de Barros BAS, de Souza Jr JP, Baumvol IJR. Iron nitride and carbonitride phases in a nitrogen implanted carbon steel. Appl Phys Lett 1982;41:237–9.
[39] Niederdrenk M, Shaaf P, Lieb K-P, Schulte O. Characterization of magnetron-sputtered ε iron-nitride films. J Alloy Comp 1996;237:81–8.
[40] Simon G, Vasconcellos MAZ, dos Santos CA. Effects of argon irradiation on a plasma-nitrided carbon steel. Surf Coat Technol 1998;102:90–6.
[41] Takahashi M, Shoji H. α″-$Fe_{16}N_2$ problem — giant magnetic moment or not. J Magn Magn Mater 2000;208:145–57.